A Novel Analytical Model as a Design Tool for Uni-Traveling-Carrier Traveling Wave Photo Detectors Approaching 1 THz

Asher Madjar, *Fellow, IEEE*, Navya Koka, Jeffry Bloch, Paul K. L. Yu, Andreas Stoehr, *Senior Member, IEEE*, and Dieter Stefan Jaeger, *Fellow, IEEE*

***Abstract*—The generation of sub-millimeter waves and terahertz signals is a difficult challenge, and a few approaches are being studied by several groups. We are investigating the approach of heterodyning two optical signals in a uni-traveling-carrier photo detector, which has been identified as the device of choice for very high frequencies. In this paper we present a novel analytical model, which was developed as a design tool for the above device. The model was validated by designing, fabricating and testing a new 100 GHz photo detector. In addition, performance limits for the UTC traveling wave photo detector are calculated by the new model, and it is shown that this device has the potential of delivering more than 1 mW of power at frequencies approaching 1 THz.**

***Index Terms*—Photo detectors, sub-millimeter wave, terahertz, uni-traveling carrier (UTC).**

I. Introduction

THE GENERATION of submillimeter waves and terahertz signals is a very difficult and yet very important task for emerging systems in imaging, spectroscopy and other applications. Several research groups are using different approaches to achieve this goal. Our approach utilizes heterodyning of two optical signals in a photo detector. During the last few years several papers have been published reporting results obtained by this approach [1]–[11]. Our study is aimed at using the above approach while maximizing output power, efficiency and frequency of operation [12]–[17]. To increase the frequency of operation one needs to use a very fast photo detector. The uni-traveling-carrier (UTC) photo detector was first presented by a group from Japan [18], and shown to be the best candidate for high frequencies. We have adopted this approach combined with the traveling wave (TW) concept.

Manuscript received April 11, 2008; revised September 22, 2008. First published December 09, 2008; current version published January 08, 2009. This work was supported in part by the Defense Advanced Research Projects Agency (DARPA) Microsystems Technology Office (MTO) via Space and Naval Warfare (SPAWAR) under Grant N66001-06-1-2022.

A. Madjar and N. Koka are with the Electrical and Computer Engineering Department, Temple University, Philadelphia, PA 19122 USA (e-mail: amadjar@temple.edu).

J. Bloch and P. K. L. Yu are with the Electrical and Computer Engineering Department, University of California at San Diego, La Jolla, CA 92103 USA.

A. Stoehr and D. S. Jaeger are with the Department of Electrical Engineering, University of Duisburg–Essen, 47057 Duisburg, Germany.

Color versions of one or more of the figures in this paper are available online at http://ieeexplore.ieee.org.

Digital Object Identifier 10.1109/TMTT.2008.2008958

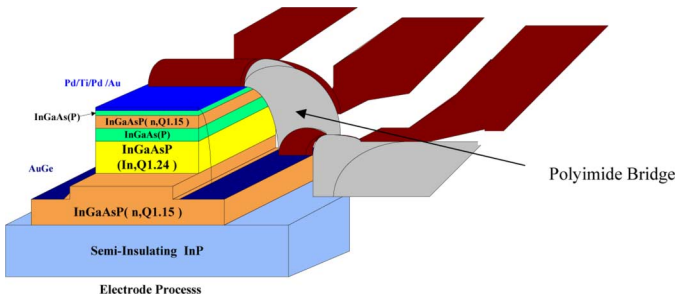

Fig. 1. Structure of UTC-TW PD (from [11]).

In this paper, we present a novel model that we have developed for the above device. The model is fully analytical and is intended to be used as a design tool. In previous publications we have presented some results based on a simplified model, which does not take into account all the physical effects. The model presented here is a full and complete model. A brief description of the photo detector is presented in Section II. The modeling approach is outlined in Section III. Simulation results of a new 100 GHz device is presented in Section IV, and the measured performance is detailed in Section V. Simulated performance limits were generated for the UTC-TW photo detector by the new model, and these are presented in Section VI.

II. UTC-TW Photo Detector

A few years ago, the UTC TW photo detector was introduced [18]. The structure of such a device is depicted in Fig. 1 [11].

This device maintains the basic structure of a TW p-i-n diode. However, there is a separation between the optical waveguide section and the absorption section. The waveguide layer is the n layer, which is transparent to 1.55-μm optical signal. The absorption layer is the p layer. The structure is designed in such a manner that most of the optical power propagates in the n layer, and only a small fraction of the power is coupled to the p absorption layer, and is absorbed there.

This device has several advantages, which are: 1) the optical power is absorbed in a distributed manner over an extended volume along the waveguide (reduced effective absorption coefficient)-increased optical saturation power and 2) since the device is reversed biased (minus in anode), the photo-generated current is composed of electrons only, which drift via the I layer into the cathode—the photo-generated holes are already in a p+ region, where they are majority carriers, which translates into a

big improvement in speed (in InP the holes are very slow compared to electrons). More details on the device are presented in [12]. As shown below, this structure has the potential to operate at frequencies of more than 300–400 GHz, at an output power of a few milliwatts and an efficiency of a few percent. An output power of around 1 mW is expected at frequencies approaching 1 THz. Such performance represents a substantial improvement of the state of the art.

III. New Modeling Approach

The new model for the UTC-TW PD is intended to be used as a design tool to predict the device performance for various dimensions and physical properties. This enables design of the device for the desired frequency, bandwidth, output power and efficiency. This also allows easy calculation of the performance sensitivity dependence on any of the physical or material properties.

To achieve this capability, it was clear from the very start that the model must be analytical, even if some accuracy is sacrificed. We succeeded in developing such an analytical model based on some reasonable approximations, which do not compromise the basic effects in the device. Some details of the model derivations are presented in the Appendix.

The derivation of the model follows these steps.

Step 1) Write down the drift-diffusion-recombination differential equations for the electron density in the absorption region. The equations include the possibility of graded doping via the introduction of a built in electric field. For simplicity we assumed a constant electric field. This is strictly correct for an exponential grading of the doping level. The inclusion of this built in E field in the model allows investigation of its effect on performance. To simplify the equations and achieve performance calculation vs. frequency, the equations were formulated in the frequency domain using the phasor approach. Thus the time dependence has been eliminated from the equations, and the equations, while still partial differential equations, they included only the spatial coordinates.

Step 2) Define the boundary conditions at the absorption-barrier interface and at the depletion-absorption interface. At the absorption/depletion interface we used the condition of zero electron density (electrons entering the I layer are swept away). At the absorption/barrier interface we used the condition of zero electron current (the barrier prevents flow of electrons). For the general case of built in electric field in the absorption region the electron current includes both drift and diffusion currents. The above condition means that at the absorption/barrier interface the drift and diffusion currents are equal, but in opposite directions

$$D_n \frac{\partial n}{\partial y} = -\mu \varepsilon n. \tag{1}$$

Step 3) Assume uniform illumination over the cross section of the absorption region (we assumed other illumination distributions as well, and the results were almost identical), and an exponential decay along the length of the device with a given effective absorption coefficient, which depends on the details of the optical design (it is possible to use a different longitudial distribution as may result from the optical design of the structure). Express the generation rate of electrons in the absorption region as function of optical power, spatial coordinates and time.

Step 4) Solve analytically the above equations for the electron density. This goal was achieved by use of the separation of variables approach. This method assumes that the electron density function is a product of three functions, each one a functions of only one spatial coordinate. Thus the partial differential equations separate into three ordinary differential equations, which can be solved analytically. This approach works well in this case, and we were able to achieve an analytical solution.

Step 5) Calculate the vertical electron current density, which is injected from the absorber into the depletion I layer (basically a diffusion current at the absorber/depletion interface)

$$J = qD_n \frac{\partial n}{\partial y}. \tag{2}$$

Step 6) Calculate the vertical electron current density along the device length taking into account the transport via the intrinsic layer. A unit charge carrier traveling via the depletion region at the saturated velocity induces a current pulse of the shape:

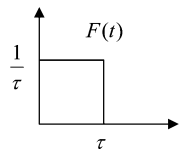

τ is the delay which is equal to the depletion layer thickness divided by the saturated velocity ($\sim 10^7$ cm/s). This is the impulse response of the depletion region. To find the electron current density after passing via the depletion region, the result from Step 5) is multiplied by the transfer function (Fourier transform of the above impulse response)

$$H(f) = \sin c(f\tau) e^{-j\pi f\tau}. \tag{3}$$

Step 7) Calculate the intrinsic device distributed capacitance (intrinsic layer capacitance). For proper operation, the depletion region must be fully depleted (by applying enough reverse bias), so the capacitance can be approximated by the parallel plate capacitance

$$C = \varepsilon (W\ L_d)/d_i. \tag{4}$$

See the Appendix for symbol definitions. The end result for the intrinsic device model is a section of

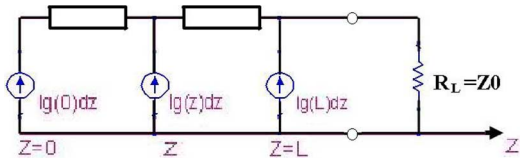

Fig. 2. Distributed model for intrinsic UTC-TW PD.

an active distributed transmission line, as depicted in Fig. 2. The model includes a distributed current source along a transmission line with a known capacitance per unit length. $z = 0$ corresponds to the input facet, and $z = L$ corresponds to the end of the device, namely, the point where the load impedance is connected (represented in Fig. 2 by the resistor R_L), which may or may not be equal to the characteristic impedance of the transmission line, Z_0. The model was implemented in MATLAB, which calculates the distributed current source and capacitance. This distributed model can be used in a circuit simulator (such as Microwave Office) to simulate the performance of the photo detector along with various microwave matching networks intended to optimize the performance for any given application.

IV. New 100-GHz Photo Detector

The new model described above was used to design a UTC-TW photo detector with an intrinsic 3-dB bandwidth of 100 GHz. The intrinsic device has the following physical parameters: absorber thickness: 0.1 μm, I layer thickness: 0.27 μm, mesa width: 2 μm, length: 27 μm. The designs were implemented by use of a coplanar waveguide structure on an InP substrate. The intrinsic device features about 100 GHz *RC* limited 3-dB bandwidth and about a 160-GHz transit time limited 3-dB bandwidth.

Design 1: Photo detector resonated by an open stub at 100 GHz including impedance transformation to enhance output power. The layout and simulated frequency response are depicted in Fig. 3(a) and (b), respectively (photo detector connected on left, probe pads on right). Vertical scale is output power in dBm. By resonating the intrinsic device capacitance one can bypass the *RC* limit, and operate at frequencies approaching the transit time limit, and even beyond. In design 1 a frequency of 100 GHz was selected. It can be seen that the expected output power at 100 GHz is about the same as for the low frequency end. This was achieved by impedance transformation.

Design 2: Photo detector with an impedance transformer at 100 GHz. The layout and simulated frequency response are depicted in Fig. 4 (photo detector connected on left, probe pads on right). Vertical scale is output power in dBm. This design features a quarter wavelength transformer intended to enhance the output power at 100 GHz. It can be seen that this design has a wider bandwidth compared to the resonant design (Design 1), and thus less sensitivity to fabrication tolerances.

V. Measured Data for the 100-GHz Device

The 100-GHz device outlined in Section IV has been fabricated and tested. The test results are presented in the following.

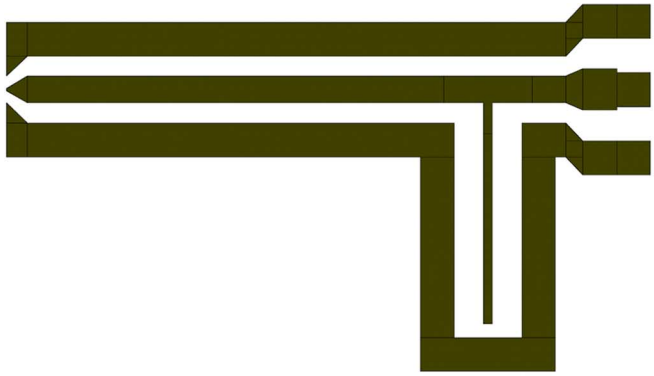

(a)

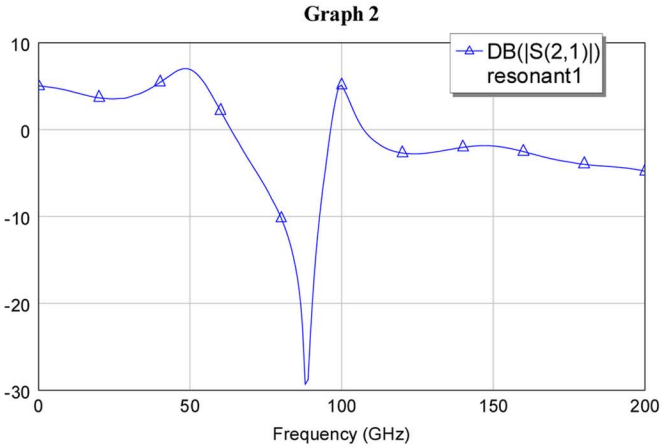

(b)

Fig. 3. (a) Layout and (b) simulated response of design 1 for 10-mW absorbed optical power.

Photographs for design 1 and 2 are depicted in Fig. 5. Unfortunately, all the devices of design 2 (transformer) were shorted out during the plating up process due to very narrow gap, as can be seen in Fig. 5(b). Thus, these devices could not be measured. The resonant devices were measured, and the results are shown below.

The frequency response of the resonant (design 1) was measured up to 110 GHz. The absolute frequency response measured by the heterodyne approach (two optical signals illuminating the photo detector simultaneously (see Fig. 6) is depicted in Fig. 7. This response demonstrates the capabilities of this device to operate beyond 100 GHz.

The graph in Fig. 7 has the same form as the simulated graph in Fig. 3(b). To get a better comparison between measurement and simulation, the two normalized frequency response curves were superimposed on the same graph. The result is depicted in Fig. 8. This result demonstrates good agreement between simulation and measurement. The main difference is the response value at the peak around 100 GHz. The measured data is a few decibels lower compared to the simulated results. This difference is attributed to a high resistance of the p contact. This conclusion was reached by measuring the S_{11} parameter of the device, and comparing to the simulated circuit data. The comparison obtained perfect match of the simulated and measured values of S_{11} for a series resistance value of 39 Ω (instead of the

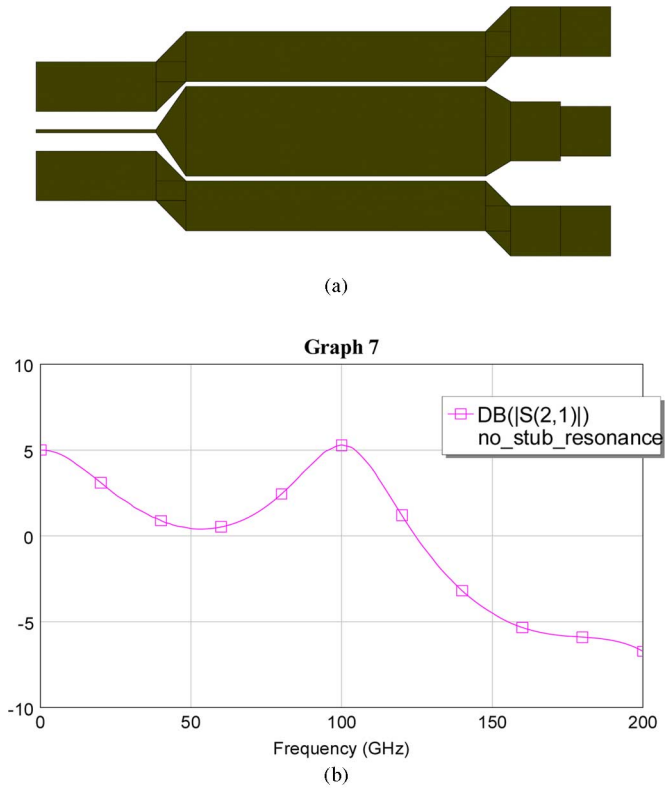

Fig. 4. (a) Layout and (b) simulated response of design 2 for 10-mW absorbed optical power.

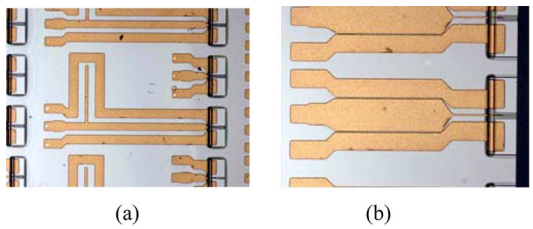

Fig. 5. (a) Resonant and (b) transformer.

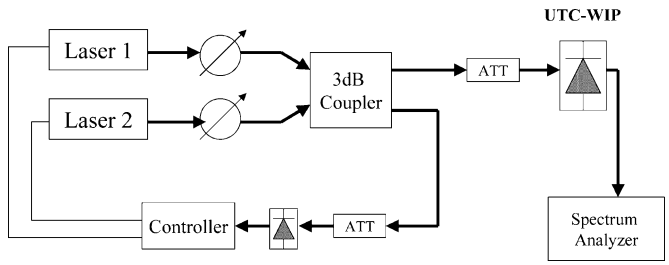

Fig. 6. Heterodyne system to measure frequency response.

design value of 10 Ω). This high value of resistance was traced to a contamination in an old evaporator used to deposit the metal for the p contact.

The simulated response of the resonant design was recalculated by using the actual value of the series resistance. The new simulation results together with the measured data are depicted

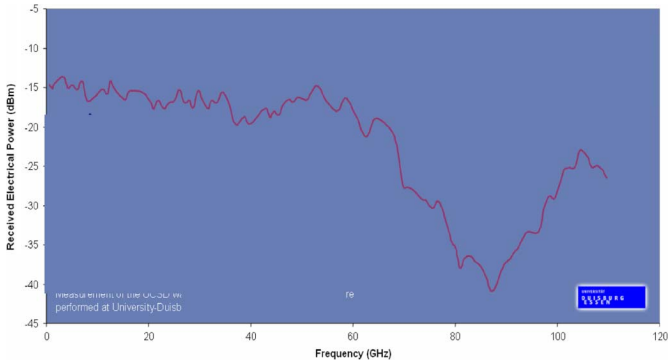

Fig. 7. Frequency response of the resonant design.

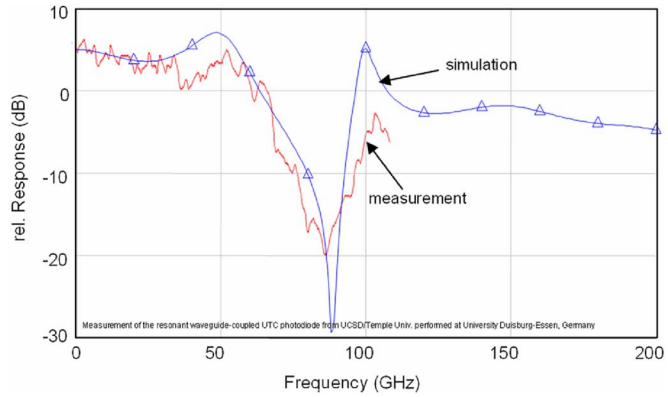

Fig. 8. Measured and simulated normalized frequency response of the resonant design.

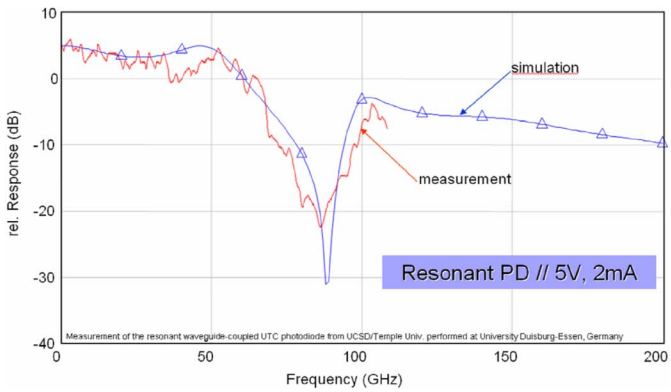

Fig. 9. Measured and simulated normalized frequency response of the resonant design with the actual series resistance and capacitance.

in Fig. 9. It can be seen that now the simulated and measured results agree very well. In addition, we can expect that a new run of these devices is going to yield a response very close to the original design.

VI. Simulated Performance Limits

In view of the results of the 100-GHz photo detector, and the reasonable correlation between measured and simulated performance, we have used the model to calculate some performance limits of the UTC-TW photo detector. The purpose is to obtain

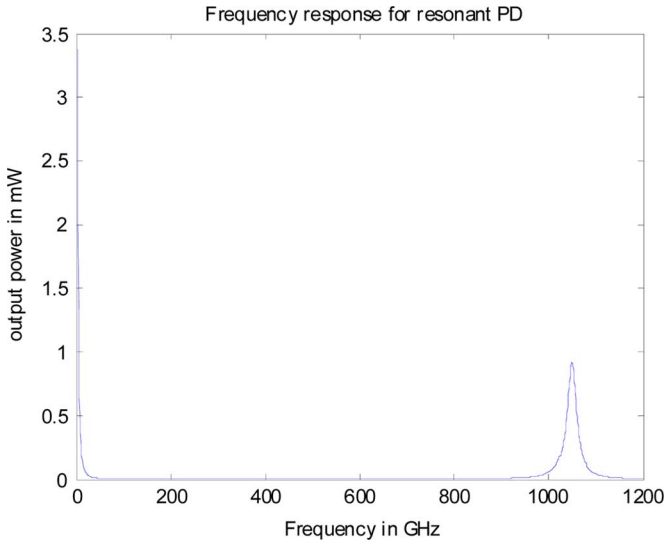

Fig. 10. Frequency response of a "next generation" PD resonated at 1 THz.

an estimate of the limits of frequency of operation (for generation of microwave signals by heterodyning two optical signals) as well as output power and efficiency.

The "next generation" PD that we have simulated has the following dimensions: absorber: 50 nm, I layer: 50 nm, mesa width: 2 μm, length: 27 μm. Simulation indicates that this device has a transit time limited 3-dB bandwidth of 800 GHz, however, the *RC* limited 3-dB bandwidth is 25 GHz. Although this device is not a practical wideband photo detector, by resonating the device capacitance, one can use it to generate signals approaching 1 THz with an instantaneous bandwidth of about 25 GHz. This is demonstrated in Fig. 10, where the frequency response is depicted for a 1-THz resonant frequency and an absorbed optical power of 10 mW and a load impedance of 50 Ω.

The above simulation indicates that even at 1 THz an output power of 1 mW is feasible. It should be noted that the above result does not take into account the microwave circuit losses. However, impedance transformation can be used to increase the load impedance, thereby increasing the output power. So, the above estimate is reasonable.

VII. Conclusion

In this paper, a novel model for the UTC-TW photo detector is presented. The model is analytical and very fast, and can be used as a design tool. The application of the model as a design tool is demonstrated by designing, fabricating and testing a photo detector operating at frequencies exceeding 100 GHz. The developed device is intended for generation of millimeter waves by heterodyning two optical signals. The model has been validated by comparing the experimental and simulated results.

Appendix

This appendix includes some details about the derivation of the new model. The cross section view of the device is depicted in Fig. 11.

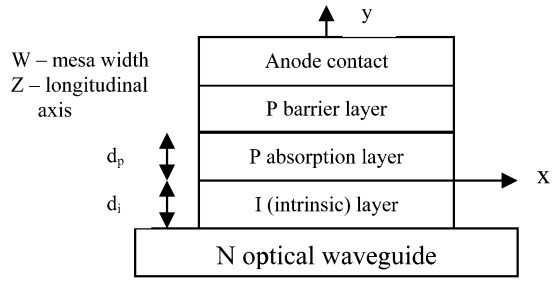

Fig. 11. Cross-section view of UTC-TW photo detector.

The analysis is performed for the reversed bias device and illuminated by two optical signals of equal amplitude and a small frequency separation ω_m

$$P_{\text{opt}} = P_o(1+\cos\omega_m t). \tag{A-1}$$

The key to the device performance is the photo generation at the absorption layer, thus the main effort of the modeling involves solution for the photo-generated electron density in the absorption region. For uniform illumination across the absorption region the generation rate of electrons

$$G_n = \frac{\alpha_e P_o(1+\cos\omega_m(t-\tau_t))}{(h\nu)Wd_p}e^{-\alpha_e z}. \tag{A-2}$$

α_e: effective absorption coefficient, $\tau_t = z/v_{\text{opt}}$: propagation delay along longitudinal (z) axis. The continuity equation

$$\frac{\partial n}{\partial t} = G_n - U_n + \frac{1}{q}\nabla J_n \tag{A-3}$$

$$U_n = \frac{n}{\tau_n} \tag{A-4}$$

$$J_n = q\mu_n n\varepsilon\hat{y} + qD_n\left(\hat{y}\frac{\partial n}{\partial y} + \hat{z}\frac{\partial n}{\partial z}\right). \tag{A-5}$$

ε is the built in electric field. Inserting all into (A-3), we get

$$\frac{\partial n}{\partial t} = G_o(1+\cos\omega_m(t-\tau))e^{-\alpha_e z} - \frac{n}{\tau_n} + D_n\left(\frac{\partial^2 n}{\partial y^2} + \frac{\partial^2 n}{\partial z^2}\right) + \mu_n\varepsilon\frac{\partial n}{\partial y} \tag{A-6}$$

where

$$G_o = \frac{\alpha_e P_o}{(h\nu)Wd_p}.$$

Express electron density as sum of dc and ac terms

$$n = N_{\text{DC}}(y,z) + \eta_m(y,z,t)$$
$$n = N_{\text{DC}}(y,z) + \eta_{mo}(y,z)\cos(\omega_m t + \theta_m). \tag{A-7}$$

Inserting (A-7) into (A-6) get the complete continuity equation, which is now separated into the following dc and ac equations.

DC equation

$$\frac{\partial^2 N_{\text{DC}}}{\partial y^2} + \frac{\partial^2 N_{\text{DC}}}{\partial z^2} + \frac{\partial N_{\text{DC}}}{\partial y}\frac{\mu_n\varepsilon}{D_n} + \frac{G_o}{D_n}e^{-\alpha_e z} - \frac{N_{\text{DC}}}{L_n^2} = 0. \tag{A-8}$$

AC equation

$$\begin{aligned}&-\omega_m\eta_{mo}\sin(\omega_m t+\theta_m)\\&=G_o\cos\omega_m(t-\tau)e^{-\alpha_e z}\\&\quad-\frac{\eta_{mo}}{\tau_n}\cos(\omega_m t+\theta_m)+\mu_n\varepsilon\frac{\partial\eta_{mo}}{\partial y}\cos(\omega_m t+\theta_m)\\&\quad+D_n\left(\frac{\partial^2\eta_{mo}}{\partial y^2}+\frac{\partial^2\eta_{mo}}{\partial z^2}\right)\cos(\omega_{mt}+\theta_m).\end{aligned}\tag{A-9}$$

As common in such analysis, we now switch to frequency domain by replacing the time domain quantities with phasors

$$\eta_{mo}\cos(\omega_{mt}+\theta_m)\longrightarrow N_{mo}e^{j\omega_m t}.\tag{A-10}$$

The final ac equation is

$$\begin{aligned}\frac{\partial^2 N_{mo}}{\partial y^2}+\frac{\partial^2 N_{mo}}{\partial z^2}+\frac{\mu\varepsilon}{D_n}\frac{\partial N_{mo}}{\partial y}-\frac{N_{mo}}{L_n^2(\omega)}\\+G_{oo}e^{-z(\alpha_e+\frac{j\omega_m}{V_{\rm opt}})}=0\end{aligned}\tag{A-11}$$

where

$$L_n(\omega)=\frac{L_n}{\sqrt{1+j\omega_m\tau_n}}\quad G_{oo}=\frac{G_0}{D_n}$$

Both equations are nonhomogeneous partial differential equations in y and z. The dc and ac equations can be solved independently. Both solutions follow the same procedure.

1) Express the complete solution as sum of the particular solution, which has the same functional form as the "driving signal" (photo-generated electrons), and the solution to the homogeneous equation.
2) Find the coefficients of the particular solution by substituting into the original equation.
3) Solve the homogeneous equation by using separation of variables: $n=n_1(y)n_2(z)$.
4) Complete the solution and find expressions for the coefficients by applying the boundary conditions.

The boundary conditions are as follows:

- $n(y=0)=0$: no electrons in depletion region.
- $(\partial n)/(\partial y)(y=d_p)=(-V_e)/(D_n)n(y=d_p)$: zero electron current across the barrier ($\mu_n\varepsilon=V_e$).

The solution to the dc equation has the following form:

$$n(y,z)=\left[A_1e^{r_1y}+A_2e^{r_2y}\right]e^{-\alpha_e z}+A_3e^{-\alpha_e z}.\tag{A-12}$$

The coefficients A_1, A_2, A_3, r_1, and r_2 are expressed in terms of the equation coefficients and boundary conditions. Equation (A-12) can be used to find the expression for the total current injected into the depletion region

$$J_n=q\mu_n n\varepsilon+qD_n\Delta n$$

at

$$y=0$$

and

$$I_{\rm DC}=\int_0^{L_d}J_nW\,dz.$$

L_d is the active region length. The expression is shown in (A-13) at the bottom of this page.

Similarly the solution to the ac equation is

$$N_{mo}=\left[B_1e^{R_1y}+B_2e^{R_2y}\right]e^{-\alpha_{ee}z}+B_3e^{-\alpha_{ee}z}.\tag{A-14}$$

$\alpha_{ee}=\alpha_e+(j\omega_m)/(V_{\rm opt})$ and the coefficients in (A-14) are expressed in terms of the coefficients in (A-11) and the boundary conditions. Note that these coefficients are complex functions of frequency, while the coefficients in (A-12) are constants. Finally the expression for the current density injected into the I region is shown in (A-15) at the bottom of this page.

The last step in the calculation of the photo-generated current density is to take into account the transit via the intrinsic layer. As explained in Section III, Step 6), this is taken care of by multiplying the current density in (A-15) by the "transfer function" of the I layer, which is expressed in (3). Further multiplying the above by the mesa width W, one gets the expression for the photo-generated current per unit length along the length of the device (z). This expression is used to calculate the distributed current source in the device model shown in Fig. 2.

$$I_{\rm DC}=qD_nA_3W\left[\frac{r_1r_2(e^{r_1d_p}-e^{r_2d_p})-\frac{V_e}{D_n}[r_1(e^{r_2d_p}-1)-r_2(e^{r_1d_p}-1)]}{(r_2e^{r_2d_p}-r_1e^{r_1d_p})+\frac{V_e}{D_n}(e^{r_2d_p}-e^{r_1d_p})}\right]\left[\frac{e^{-\alpha_e L_d}-1}{-\alpha_e}\right]\tag{A-13}$$

$$J_n=qD_nA_3e^{-\alpha_{ee}z}\left[\frac{R_1R_2(e^{R_1d_p}-e^{R_2d_p})-\frac{V_e}{D_n}[R_1(e^{R_2d_p}-1)-R_2(e^{R_1d_p}-1)]}{(R_2e^{r_2d_p}-R_1e^{r_1d_p})+\frac{V_e}{D_n}(e^{R2d_p}-e^{R_1d_p})}\right]\tag{A-15}$$

REFERENCES

[1] A. Stöhr *et al.*, "Ultra-wideband traveling-wave photodetectors for photonic local oscillators," *J. Lightw. Technol.*, vol. 21, no. 12, pp. 3062–3070, Dec. 2003.

[2] A. Stohr *et al.*, "THz photomixing employing traveling-wave photodetectors," in *IEEE MTT-S Int. Microw. Symp. Dig.*, Fort Worth, TX, Jun. 2004.

[3] A. Malcoci *et al.*, "Optical submillimeter-wave generation employing antenna integrated ultra-fast traveling-wave 1.55 μm photodetectors," in *IEEE MTT-S Int. Microw. Symp. Dig.*, Philadelphia, PA, Jun. 2003.

[4] M. Alles *et al.*, "High-speed traveling-wave photodetectors for . . .," in *Asia–Pacific Microw. Conf.*, 1997.

[5] A. Stohr *et al.*, "Integrated photonic THz transmitter employing ultra-broadband . . .," in *Microw. Photon. Meeting*, 2002.

[6] P. D. Grant, H. C. Liu, and R. Dudek, "MM wave mixing in a quantum well IR photodetector," in *IEEE MTT-S Int. Microw. Symp. Dig.*, Philadelphia, PA, Jun. 2003.

[7] E. Peytavit *et al.*, "An ultra-wide bandwidth photomixer with down conversion at terahertz frequencies," in *Proc. 10th IEEE Int. Terahertz Electron. Conf.*, 2002.

[8] P. G. Hugard *et al.*, "Efficient generation of guided millimeter wave power by photomixing," *IEEE Photon. Technol. Lett.*, vol. 14, no. 2, pp. 197–199, Feb. 2002.

[9] T. Chau *et al.*, "Generation of millimeter waves by photomixing at 1.55 μm using InGaAs–InAIAs–InP velocity-matched distributed photodetectors," *IEEE Photon. Technol. Lett.*, vol. 12, no. 8, pp. 1055–1057, Aug. 2000.

[10] P. G. Huggard *et al.*, "Generation of milimetre and sub-millimetre waves by photomixing . . .," *Electron. Lett.*, Mar. 2002.

[11] T. S. Liao, P. Mages, and P. K. L. Yu, "Integration of the high-power integrated uni-traveling carrier and waveguide integrated photodiode," in *IEEE MTT-S Int. Microw. Symp. Dig.*, Philadelphia, PA, Jun. 2003.

[12] A. Madjar, P. R. Herczfeld, A. Rosen, P. Yu, and D. Jager, "Design considerations for a uni-traveling carrier traveling wave photo detector for efficient generation of millimeter wave and sub-mm wave signals," in *Eur. Microw. Conf.*, Paris, France, Oct. 2005.

[13] A. Madjar, T. S. Liao, and P. Yu, "Possible efficient generation of sub-mm wave signals by heterodyning two optical signals in a UTC-TW photo detector," in *Proc. Eur. Microw. Conf.*, Manchester, U.K., Sep. 2006.

[14] A. Madjar and T. Berceli, "Microwave generation by optical techniques—A review," in *Proc. Eur. Microw. Conf.*, Manchester, U.K., Sep. 2006.

[15] A. Madjar, N. Koka, M. Draa, J. Bloch, and P. K. L. Yu, "Bandwidth reduction of UTC-TW photo detector at high optical power levels," in *IEEE MTT-S Int. Microw. Symp. Dig.*, Honolulu, HI, Jun. 2007, pp. 2193–2196.

[16] A. Madjar and P. K. L. Yu, "The potential of high speed UTC-TW photo detectors to generate sub-mm wavesignals—Predictions by a new analytical model," in *IEEE/LEOS Summer Opt. Freq. Time Meas. Generation Topical Meeting*, Portland, OR, Jul. 23–25, 2007.

[17] A. Madjar, N. Koka, J. Bloch, M. Draa, and P. M. L. Yu, "A novel analytical model for the UTC-TW photo detector for generation of sub-mm wave signals," in *Proc. Eur. Microw. Conf.*, Munich, Germany, Oct. 2007.

[18] T. Ishibashi, N. Shimizu, S. Kodama, H. Ito, T. Nagatsuma, and T. Furuta, "Uni-traveling carrier photodiodes," *Ultrafast Electron. Opto-electron.*.

Asher Madjar (M'73–SM'83–F'97) received the B.Sc. and M.Sc. degrees from the Technion, Israel Institute of Technology, Haifa, Israel, in 1967 and 1969, respectively, and the D.Sc. degree from Washington University, St. Louis, MO, in 1979.

From 1969 to 2003, he has been with RAFAEL, Haifa, Israel, and with the Technion. From 1989 to 1991, he was a Visiting Professor with Drexel University, Philadelphia, PA. He is currently a Research Professor with Temple University, Philadelphia, PA. He has authored or coauthored over 150 papers. He is on the Editorial Review Board of *Microwave Journal*.

Dr. Madjar served as the Israel IEEE Antennas and Propagation (AP)/Microwave Theory and Techniques (MTT) Chapter chairman for several years, and in that capacity organized 15 symposia. He serves as a member of the Management Committee and Technical Program Committee of the European Microwave Conference. He served as the chairman of the 27th European Microwave Conference, Jerusalem, Israel (1997). He is on the Editorial Review Board of the IEEE TRANSACTIONS ON MICROWAVE THEORY AND TECHNIQUES and IEEE MICROWAVE AND GUIDED WAVE LETTERS. He was the recipient of the 1998 Rafael Best Researcher Prize.

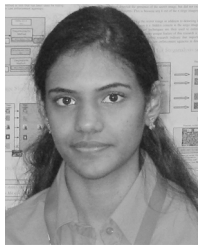

Navya Koka received the Bachelors of Technology degree from Nagarjuna University, Nagarjuna, India, in 2005, and the Masters of Science degree from Temple University, Philadelphia, PA, in 2008.

She has authored or coauthored several papers related to her M.Sc. thesis project. She is currently a Microwave Design Engineer.

Ms. Koka is a member of IMAPS.

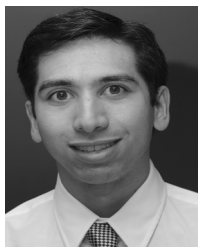

Jeffrey Bloch received the B.Sc. degree in electrical engineering from Brown University, Providence, RI, in 2003, and is currently working toward the Ph.D. degree at the University of California at San Diego, La Jolla.

His current research focuses on wide bandwidth high-power photo detectors for fiber-optic links.

Paul K. L. Yu is currently a Professor with the Department of Electrical and Computer Engineering, University of California at San Diego (UCSD), La Jolla.

With UCSD, he conducts research on semiconductor materials and devices for various photonics and microwave photonics applications. His research interests include lasers in the near-infrared wavelength region for optical communication and optical interconnection, optical/RF modulation schemes for narrowband high center frequency microwave transmission, high-speed high-power optical detectors and high-speed waveguide modulator devices for both digital and analog modulations, and high-power semiconductor optical switches for microwave generation.

Prof. Yu is a Fellow of the Optical Society of America.

Andreas Stöhr (M'97–SM'07) received the Dipl.-Ing. and Dr.-Ing. degree in electrical engineering from Gerhard-Mercator-University Duisburg (GMUD), Duisburg, Germany, in 1991 and 1997, respectively.

Since 1995, he has been a member of ZHO-Optoelektronik, Universität Duisburg–Essen, Duisburg, Germany. In 1998 and 1999, he joined Japan's Communications Research Laboratory (CRL), Ministry of Posts and Telecommunications. He is currently engaged in advanced and ultrafast photonic components for optical millimeter-wave and terahertz generation. He is also active in the field of broadband millimeter-wave photonic wireless systems using radio-over-fiber (RoF) techniques. His current research interests include the design and fabrication of III/V-based microwave photonic devices and their application in microwave or millimeter-wave fiber-optic transmission systems, as well as in optical sensors. He has authored or coauthored over 100 papers in refereed journals and conferences.

Dr. Stöhr was a conference chair of the Photonics Europe–Millimeterwave and Terahertz Photonics Conference. For many years, he has served as a Technical Program Committee (TPC) member for many international conferences including the International Topical Meeting on Microwave Photonics and the LEOS annual meeting.. He is a senior member of the IEEE Laser and Electro-

Optic Society (LEOS) and also a member of the IEEE Microwave Theory and Techniques Society (IEEE MTT-S). He was the recipient of the 1997 Annual Award presented by the DUG.

Dieter Stefan Jäger (F'01) received the Diplomphysiker, Dr.rer.nat., and Habilitation degrees in physics from the University of Münster, Münster, Germany, in 1969, 1974, and 1980, respectively.

Since 1990, he has been with the Faculty of Electrical Engineering, University of Duisburg (now the University of Duisburg–Essen), where he is Head of the Department of Optoelectronics. He was Dean of the Faculty of Electrical Engineering from 1998 to 2001. He has authored or coauthored over 400 papers in books, journals, and conference proceedings. He is an Honorary Professor of Brasov University, Brasov, Romania, Consultant Professor of the Huazhong University of Science and Technology, Wuhan, China, and Consultant of Construction Consultant Committee of Wuhan-Optics Valley of China. He is consultant of the IEE Photonics Network, London, U.K., a member of the Photonics Competence Center, Frankfurt, Germany, and founder of OpTech-Net, a German Network of Excellence on optical technologies, Duisburg, Germany, and a member of the International Coalition of Optoelectronic Industry Association (ICO). He is currently engaged in nonlinear phenomena in solid-state devices where he is mainly concerned with nonlinear microwaves for MMIC applications, as well as nonlinear optics, ultrafast and terahertz electrooptics, and optical switching in semiconductors for opto-electronic signal processing. His research interests include ultrafast opto-electronics for microwave power generation and transmission, millimeter-wave optical links for broadband communication technologies, polymer optical links for home networks, and picosecond electrooptical measuring techniques. He is also active in the areas of terahertz technology, solar cells using nanoparticles, optical neural technology, and opto-electronics for medical applications.

Prof. Jäger is chair of the German IEEE Lasers and Electro-Optics Society (LEOS) Chapter. He is a member of the IEEE Microwave Photonics Steering Committee. He was a LEOS Distinguished Lecturer (2004–2005).